Experimental Investigation on the Impact of different Thermodynamic Parameters on the Depletion Behavior of Nuclear Aerosols in the IN-EX Facility

Y. Wu[1], M. Klauck[2,*], H.-J. Allelein[1,2]
[1]RWTH Aachen University, 52056 Aachen, Germany
[2]Forschungszentrum Jülich GmbH, 52425 Jülich, Germany
[*]Corresponding author: m.klauck@fz-juelich.de

Abstract

Fission products (FPs) released in the process of a severe loss of coolant accident can reach the containment – the last barrier against the leakage of radioactive isotopes to the surrounding environment – as airborne particles. Consequently, reliable assessment of a potential radiological source term requires in-depth knowledge of the aerosol behavior. The IN-EX facility at Forschungszentrum Jülich (FZJ, Germany) is built to study nuclear aerosol depletion behavior under accident scenarios by varying thermodynamic parameters (relative humidity, temperature and pressure). We performed a series of experiments using both, pure and mixed particles. The objective is to improve the understanding of aerosol depletion mechanisms and provide the latest data for optimization and validation of computational models for aerosol behavior.

In the IN-EX experiments, SnO_2 and CsI represent the insoluble and soluble particles released from the damaged core, respectively. In the case of mixed particles, in order to figure out the effect of varying mass composition on the aerosol behavior, we used the mass compositions of CsI and SnO_2 in the ratio of 3:7 and 6:4 in this paper. In this work, we measured the mass concentration and size distribution, and derived the corresponding aerosol removal rate to analyze the data. During the experiments on CsI aerosols, we observed that the aerosol removal rate is accelerated by an increase in relative humidity, while relative humidity seems to have no effect on the depletion of SnO_2 aerosol. Furthermore, pressure or temperature appears to have no significant effect on the depletion behavior both of SnO_2 and CsI aerosols. Combining with the results of pure substances, we investigated the regularity of the depletion behavior of mixed aerosols. In general, SnO_2 has the highest aerosol removal rate, while CsI has the lowest one. The aerosol removal rate of the mixture is between SnO_2 and CsI. The components in the mixture with a high mass fraction determine the depletion behavior of this mixture. Particularly in the condensed state, we found almost no difference in the aerosol removal rate of either pure substances or mixtures.

Keywords: severe accident, experimental research, aerosol depletion behavior, mixed aerosol

1 Introduction

As a result of a severe loss of coolant accident (LOCA), the core will degrade and FPs will be released into the containment, especially in the event of a subsequent vessel failure. During the release, radioactive particles will be carried by gases (e.g., steam and non-condensable gas) and combined to form aerosols. Minimizing the spread of radioactive materials to the environment in severe accidents is the main objective of reactor safety research. Some studies on aerosol behavior focus on how to benefit aerosol retention after a severe accident (SA) to reduce the impact of radioactivity on the environment and human health. With some researchers focusing on the depletion behavior of aerosols, multi-component aerosol is one of the priorities of these studies [1]. Depletion behavior studies contribute to our understanding of accidental aerosols mechanisms specifically during both, the IN- and EX-Vessel phase.

Over the last decades, a series of experiments have been carried out on aerosol depletion behavior, especially from projects DEMONA, VANAM and KAEVER. The DEMONA tests in 1987 were the first large-scale tests on tin dioxide (SnO_2) aerosol depletion in the 640 m^3 Battelle model containment (BMC). These experiments provided experimental data for the development of computational codes for aerosol behavior [2, 3]. In 1991, advanced tests of the VANAM series were performed on mixed condensation aerosols in the BMC based on DEMONA but under different thermohydraulic conditions [4, 5], focusing mostly on the multi-compartment geometry impact. In the KAEVER project in 1997, experiments were carried out with advanced instrumentation to study the influence of relative humidity on aerosol depletion behavior [6, 7, 8, 9]. The results were applied to simulate and validate computational models of aerosol behavior at that time, and it was subject of the International Standard Problem ISP 44 [6]. The important results from these projects are that deposition is strongly affected by material hygroscopicity and atmospheric humidity [3]. However, several details about aerosol behavior, especially aerosol mechanism, have remained unclear. Due to the limited preservation of experimental data over the last decades, conducting new experimental work using advanced instrumentation is essential. These experimental data could extend the database for validation and improve the computational programming. In addition, up to now hardly any attention has been paid to the effect of pressure on aerosols [1].

The PHÉBUS FPT2 results from hot leg samples showed that the gaseous Cs portion is less than 6 %; hence most of the Cs are transported in the primary circuit in the form of aerosols, particularly mainly as multi-component aerosols [10, 11]. The composition of the aerosol depends on the degradation stage. The highest aerosol concentrations are found in the bundle oxidation stage, when Ag, In, Cd and Sn are predominant. Subsequently, in the final degradation stage, with the formation of the melt pool, the aerosol becomes Ag, Re, Cs and Mo, followed by Ag, Re, and U [12]. The composition of the source term released into the containment in FPT3 was dominated on average by the fission product noble gases, the volatile FPs Cs and Mo (around 56 % in total), the structural material Sn from the fuel cladding (around 13 %), the control rod material Ag, In, Cd and B, W and Re from thermocouples (around 10 %), then other volatile FPs (around 5 %) such as Te, Rb and I, the lower volatile Ba and the fuel material U [11]. In the IN-EX experiments, we discussed with other experts and decided to take CsI and SnO_2 as representative soluble and insoluble nuclear aerosols.

In this paper, systematic experiments on the depletion behavior of mixed aerosols were conducted on the effects of thermodynamic parameters – relative humidity, temperature, and pressure – using the IN-EX facility. The size distribution and particle concentration are measured by a cascade impactor (Electrical Low Pressure Impactor – ELPI+). The experimental data contribute to a better understanding of the aerosol depletion behavior. The results could not only be instructive for Probabilistic Safety Assessment (PSA), but could also be applied for the improvement and further validation of aerosol behavior models.

2 Experimental program

The IN-EX facility at FZJ is built to simulate the thermophysical boundary conditions in a LWR containment and investigate the impact of a variety of thermodynamic conditions such as pressure, temperature and relative humidity. This facility can be applied to study different phenomena of severe accident aerosols, such as pool scrubbing, depletion, and interaction behavior. Table 1 illustrates the design specifications in detail. The IN-EX facility contains a pressure vessel, an aerosol conditioning line and three aerosol generators, which are Powder Dispersing with a Brush (PDB), Air Atomizing Spray Nozzle System (ASNS), and Cable Fire Aerosol Generator (CFAG). The CFAG is designed for generating cable fire products (CFP), but it is not the topic of this paper. More information about the CFAG was published by Allelein et al. [13].

2.1 IN-EX Vessel

The main component of the IN-EX facility is the pressure vessel shown in Figure 1. The vessel can be operated under a maximum gauge pressure of 8 bar (g) and a maximum temperature of 200 °C. The vessel has a free internal volume of 1.08 m^3 with a 2 m height and an 800 mm diameter. In order

Table 1: Design parameters of IN-EX facility.

Parameter	Content
atmosphere composition	nitrogen, steam, air, helium
Humidity	$0\% - 100\%$ RH and condensation conditions
Operational temperature	max. 200 °C
Operational pressure	max. 8 bar (g)
Height	2 m
Diameter	800 mm
Insoluble aerosol species	SnO_2, Ag
Soluble aerosol species	$CsOH$, CsI, Cs_2MoO_4, $NaCl$
Particle size distribution	$0.1 - 10$ µm
Particle concentration	$0.1 - 5$ g/m^3

to maintain operating temperatures for the IN-EX vessel, insulation with electrical heaters is installed outside to reduce heat losses and to avoid the impacts of temperature fluctuation. A total of eleven sheathed thermocouples type T are installed in various positions throughout the vessel with a standard accuracy of $\pm$ 1 °C according to the manufacturer. Three of them are attached on the inner wall to determine the wall temperature. Three more are used to measure the gas temperature near the inner wall. This allows us to characterize the difference between the wall and the gas temperature near the wall. The remaining five are used to determine the gas temperature in the center, which gives the temperature distribution in the vessel. In addition to the temperature, the pressure in the IN-EX vessel is controlled by a PID control valve, measured by a pressure sensor. The relative humidity is provided by a steam generator and measured by capacitive humidity sensor with $\pm$ 0.2 % r.h. measuring accuracy.

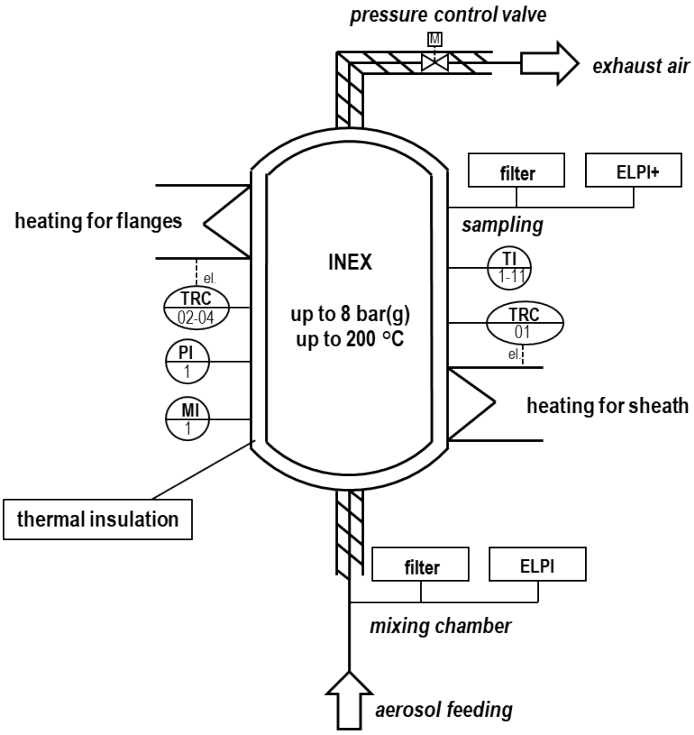

Figure 1: IN-EX pressure vessel.

2.2 Aerosol generation

An advanced PDB is installed to generate insoluble aerosols such as SnO_2 and Ag. By control from the pellet feed velocity, the initial concentration of the inlet aerosol is maintained constant. The ASNS

is suitable for generating soluble particles such as CsI. Ensuring a constant flow rate of the solution in the nozzle, the initial concentration remains constant. Details about these two generators were described by Krupa et al. [14]. Both of PDB and ASNS show stable and reproducible generation profiles in experiments (Figure 2). In the experiments, the effective aerodynamic particle diameters are generated in the range of 0.3 µm to 3 µm. The relative deviation from aerosol generator regarding the number concentration is around 0.68 to 0.27 for PDB and 0.13 to 0.37 for ASNS depending on the particle size class.

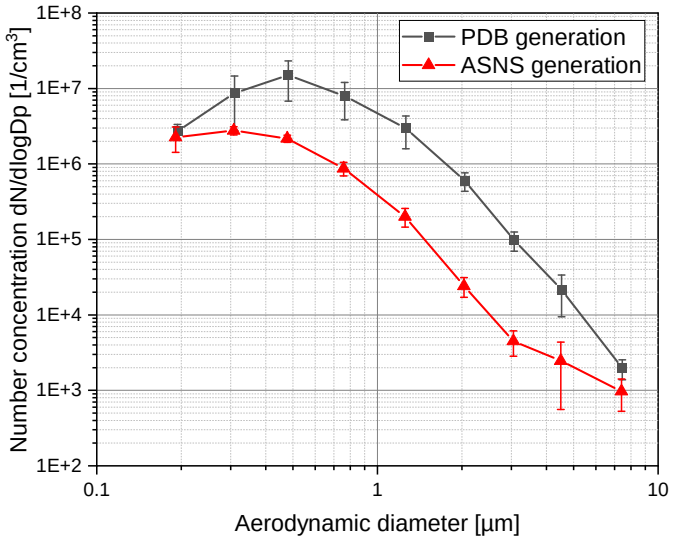

Figure 2: Generation profiles of PDB and ASNS.

It is clear that in our experiments the initial particle sizes of the soluble and insoluble particles were not identical. The initial particle size distribution does influence the particle growth process and in turn changes the cumulative mass concentration. However, it is very difficult to ensure that the initial size distribution between soluble and insoluble particles is the same. Differences in particle size distribution are not only seen between soluble and insoluble particles, but also between different projects for the same species. This makes it difficult to compare experimental data between different projects. Based on this, we tried to verify in our experiments that it is possible to compare the depletion behavior of particles even if they have different initial size distributions. In our experiments, we are concerned with the summed changes of different particle sizes and the size distribution of the particles helps us to analyze the particle mechanism during depletion. The mathematical derivation of the concentration changes has been validated for a long time, and depletion trends are not the focus of our paper; the aerosol removal rate comparison under different temperature/pressure/relative humidity at the same depletion time is the vital points in our paper. Furthermore, we cannot claim that the particle size distribution in our experiments is the same as that in severe accidents. However, these results at least help us to get closer to the real situation.

In this work, the Reynolds number of particles is less than 1.0, indicating that the particles are surrounded by laminar flow and their viscous forces are much larger than inertial forces [15]. The particles are located in the Stokes's region and are mainly subject to drag forces, meaning the motion of the particles follows the Stokes's law. The particle motion following the Newton's law as Reynolds number beyond 1.0 is not discussed in this work. The Reynolds number of particles can be calculated by equation 1, when particle density ρ_p, settling velocity v_s and dynamic viscosity η are known. The particle Reynolds number of the experiments in this paper are illustrated in Table 2. In the calculation the effective density, i.e., half of the bulk density, is estimated as particle density in the case of converting the equivalent Stokes's diameter [16].

$$Re_p = \frac{\rho_p v_s d_p}{\eta} \tag{1}$$

Table 2: Particle Reynolds number of SnO_2, CsI and their mixture in the particle diameter range of 0.3 µm to 3 µm at the standard conditions (1 atm, 20 °C) .

Type of particle	Effective density	Particle Reynolds number
SnO_2	3500 $\mathrm{kg\,m^{-3}}$	0.006 - 0.58
CsI	2250 $\mathrm{kg\,m^{-3}}$	0.002 - 0.24
Mixture	3000 $\mathrm{kg\,m^{-3}}$	0.004 - 0.43

2.3 Test procedure

The test procedure of the aerosol depletion experiments is divided into 4 steps in total: flushing, pre-conditioning (pre-heating, pre-pressurizing and pre-humidification), injection and depletion.

Flushing : Before each experiment, the IN-EX vessel is flushed overnight with compressed air at a volume flow of 20 $\mathrm{m^3\,h^{-1}}$: This ensures that the particles remaining in the vessel due to deposition and sedimentation from the previous test are carried out of the tank, which ensures that the initial conditions, especially the particle concentration are similar for each experiment.

Pre-conditioning: The boundary conditions of each test such as temperature, relative humidity and pressure are set to the desired conditions prior to the injection of the aerosol.

Pre-heating: First, the vessel is preheated to the conditions required for the experiment. The heating temperature can be set by the electric heating system outside the vessel to a maximum of 200 °C. The desired heating and test temperature is set to room temperature around 23 °C (without heating), 60 °C, 120 °C and 180 °C. This is consistent with the temperature setting of the cascade impactor. As shown in Figure 3, TRC5101 is the heating temperature, TI5106 is the main gas temperature and TI5001 is the inner wall temperature measured by the thermocouple in the vessel. The temperature in the vessel is shown as a constant after the injection phase. The temperature difference between wall and main gas is less than 3 °C. Since this temperature difference is slight and occurs in every test, therefore, we ignored the effect of thermophoresis to aerosol deposition behavior in our experiments. Due to the thermal conductivity of the vessel wall and the heat transfer of the gas inside the vessel, the gas temperature inside the Tank is approx. 10 °C lower than the heating temperature.

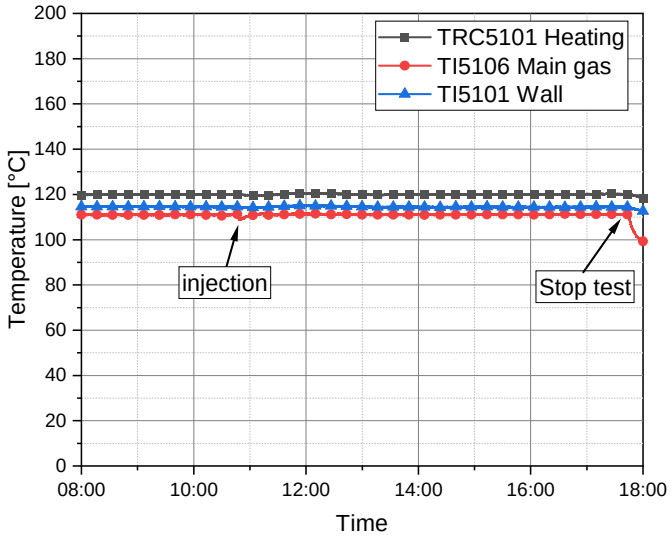

Figure 3: Measured Temperature change during the test from heating controller TRC5101 and thermocouple TI5108 for gas (heating temperature is set as 120 °C).

***Pre-pressurizing*:** Prior to the injection phase, nitrogen is injected at a volume flow rate of 20 $\mathrm{m^3\,h^{-1}}$ to bring the pressure up to the experimental conditions. The maximum operating pressure of the vessel is 8 bar (g). A PID control valve keeps the pressure constant. The pressure settings used for the experiments are atmospheric pressure (0 bar (g) without nitrogen pre-injection), 3 bar (g) and 6 bar (g). It should

be noted that there is a difference between the atmospheric pressure experiments and the higher pressure experiments. With the former being an open system and the latter being a closed system. This means that a pressure drop due to particle sampling during the measurement cannot be avoided in a closed system.

Pre-humidification: In order to meet the desired humidity conditions, a steam generator is used to change the relative humidity inside the vessel. Since relative humidity is highly related to temperature, setting a high relative humidity at high temperatures at the same time requires the provision of a disproportionately large amount of water, which is not easily achieved with existing equipment peripherals. Therefore, the experimental temperature of CsI is set to 60 °C to be able to vary the relative humidity from dry to condensation conditions. Furthermore, the resistance to steam injection increases due to the back-pressure from the pressurized vessel. This poses additional difficulties for the steam generator. Hence, precise control of the relative humidity in the IN-EX vessel cannot be achieved. In the IN-EX experiment, the non-injected steam is simulated as a dry condition. As shown in Figure 4, during the steam injection, if the relative humidity reaches the desired value, the steam injection stops and the aerosol injection continues. Under condensation conditions, the steam does not stop until the aerosol injection is complete. The condensation state is maintained during the depletion phase, as the atmosphere in the vessel will remain still after stopping the injection and no water will be lost unless deposited. The boundary conditions for the variation of the moisture content are defined as: "dry" (r.h. $\leq$ 30 %), "medium humidity" (30 % < r.h. $\leq$ 80 %), "high humidity" (80 % < r.h. $\leq$ 100 %) and "condensation" (r.h. > 100 %).

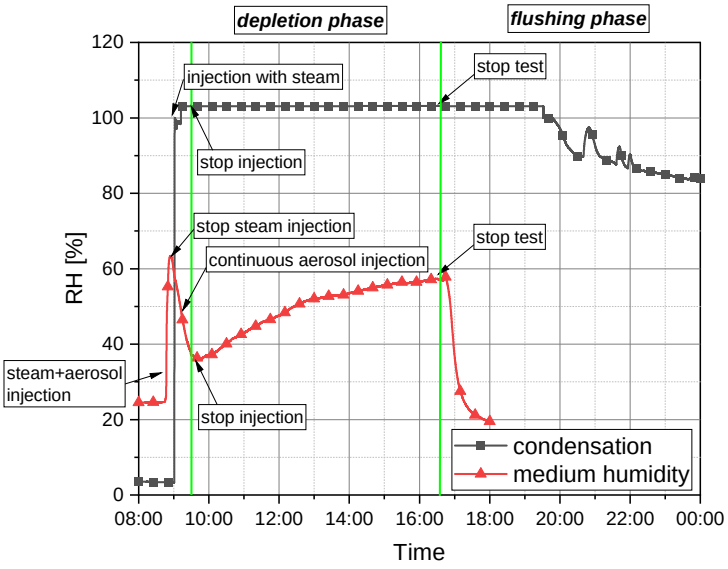

Figure 4: Relative humidity change during the test under condensation and medium humidity.

Injection: Once temperature, pressure, and relative humidity inside the IN-EX vessel are at test conditions, the aerosol injection phase starts. To be able to compare the results, particle generation (ASNS and PDB) and injection procedure are kept consistent in all experiments. The CsI particle solution (around 34.9 %) as a representative of soluble particles is fed into the vessel by ASNS, or SnO_2 particles (representing insoluble particles) generated by PDB are injected into the tank. As shown in Table 3, the mass composition of these two types of particles depends mainly on the PDB settings. The carrier gas is the non-condensable gas nitrogen (N_2). Its flow rate is always maintained at a total of 20 $m^3 h^{-1}$, and the injection phase lasts for 30 min in each experiment, leading to particle number concentrations up to 10^7.

Depletion phase: After injection of the aerosol, the depletion behavior is observed and the necessary parameters such as particle concentration and size distribution are measured with ELPI+. The ELPI+ is a type of cascade impactor and enables real-time detection of particles by combining electrical detection of charged particles with a low voltage cascade impactor [17]. Avoiding overloading effect of the ELPI+ sampling is in consideration during measurements. In order to ensure a high measuring accuracy of the ELPI+, a double diluter system by company Dekati is used for diluting aerosol before entering the ELPI+.

Table 3: Injection parameters in the experiments for pure substances and their mixtures.

Mass composition CsI:SnO_2	ASNS (solution mass flow)	PDB (particle mass flow)
1:0	250 $g\,h^{-1}$	-
6:4	245 $g\,h^{-1}$	56.65 $g\,h^{-1}$
3:7	250 $g\,h^{-1}$	207.73 $g\,h^{-1}$
0:1	-	377.66 $g\,h^{-1}$

There are two types of diluters: Dekati Diluter DI-1000 and the high pressure Diluter DEED-300. Both were applied in the experiments. The DI-1000 is suitable for ambient conditions and the DEED-300 for high pressure experiments. The dilution factor is controlled by the flow rate of the dilution air. The total depletion time of each test is 8 hours, with an average of 10 minutes for each single sampling period. As shown in Figure 5, there is one measurement every 2 hours after the end of the injection process. However, during the initial 2-hour depletion period, there are 2 more measurements. Since it was known from pretests that there is a strong depletion behavior during the initial phase. Including the injection measuring, 7 measurements are carried out during the 8-hour depletion phase in total.

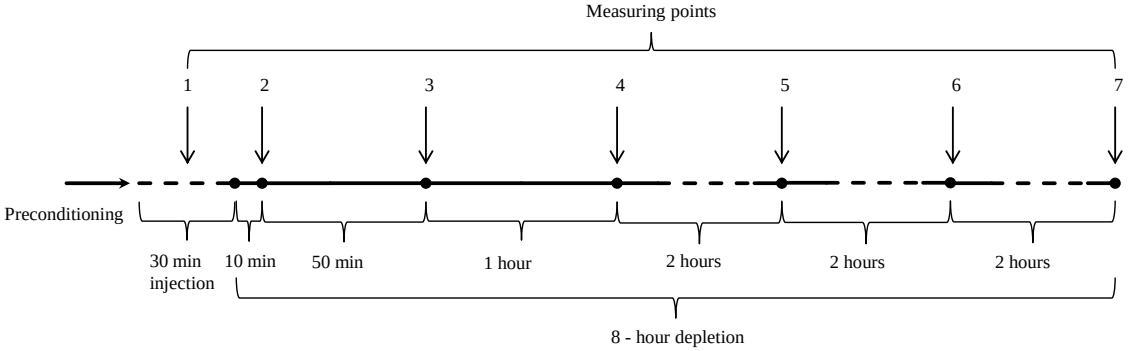

Figure 5: Timeline of experiments.

3 Results and discussion

In the aerosol depletion experiments two aspects of the results are of specific interest. Firstly, the change in aerosol concentration, especially the mass concentration, during the 8 hours of depletion is investigated. Secondly, the change in size distribution of the aerosols is also of interest in the experiments. The comparison of mass concentrations and particle size distributions at the same depletion time point under different thermodynamic parameters is the main task of the IN-EX experiment. In this work, systematic experiments from pure aerosols to multi-component aerosols were performed. The study of the depletion behavior of pure SnO_2 and CsI aerosols is essential to further understand the mechanisms of aerosols in severe accidents. It provides the basis for the analysis of multi-component aerosols results. To simulate the representative nuclear aerosol composition, or as close as possible, the mass composition of CsI and SnO_2 was set to 6:4 in this paper [11, 12]. The other mass composition of CsI and SnO_2 with 3:7 are used as comparison tests. Thus, IN-EX experiments can obtain general properties of the depletion behavior of mixtures with different mass compositions. During the analysis of the particle mechanisms, thermophoresis is neglected because of the slightly temperature difference between wall and main gas. In our experiments, agglomeration and sedimentation are the two concerned mechanisms affecting particle size distribution and mass concentration.

In comparison with results from other works, we found that mass concentration-time plots were used to describe depletion behavior. However, as mentioned previously, comparing mass concentration data among different projects is challenging as different test rigs have various designs. In particular, the magnitude of the measured initial injection mass concentration is different since the size and dimensions of the experimental vessels vary from project to project. As shown in Table 3, the initial concentration

is even different in our experiments with various mass compositions. Moreover, the injection mass flow rates are not necessarily comparable between various projects. For data comparison with other works, a suitable way to verify the experimental data is to shift the mass concentration-time plot to the right or to the left to find similar mass concentration magnitudes as other experiments. However, shifting is firstly rough, which can only qualitatively validate the data. Secondly, after shifting, the depletion time seems to be worthless in this case because the X-axis is also relocated with it. Therefore, in order to be able to compare results between different vessels and projects, even at different injection conditions, especially when the initial mass concentration varies considerably, it is necessary to define a parameter to describe the depletion behavior to make quantitative comparisons possible, taking into account the effect of depletion time.

Aerosol removal rate λ is defined to describe the rate of mass concentration decay during the depletion process compared to the initial mass concentration by equation 2. The product of aerosol removal rate and effective height of particle cloud λh represents an effective deposition velocity [15, 18]. Typically to obtain λ in a mathematically way, the size distribution function must be solved or known [18]. Otherwise λ can be specified from the experimental data, expressed in equation 4, which comes from the equation 3. The Aerosol removal rate emphasizes the effect of time on depletion behavior and makes it possible to compare data with different initial mass concentrations quantitatively on the same time axis.

$$\frac{dm}{dt} = -\lambda(t)m(t) \tag{2}$$

$$m(t) = m_0 e^{-\lambda t} \tag{3}$$

$$\lambda = -\frac{ln\frac{m(t)}{m_0}}{t} = \frac{lnm_0 - lnm(t)}{t} \tag{4}$$

The deposition rate R is another parameter which can be used to compare the particle depletion behavior in various thermodynamic parameters. The deposition rate R can be calculated based on the Equation 5 from COCOSYS [16]. v_{TS}, v_{diff}, v_{dph} and v_{th} are terminal settling velocity, diffusion velocity, diffusiophoresis velocity and thermophoretic velocity, corresponding deposition processes. The sedimentation velocity v_{TS} is calculated by means of Stokes' formula [19]. h is here effective deposition height. Sedimentation is considered to be the dominant deposition process in IN-EX experiments. As the particles focused in this work are in the range between 0.3 µm and 3 µm, the effect of diffusive deposition can be neglected. The IN-EX vessel has well maintained temperature properties and thermophoresis can also be neglected. It should be noted that in the condensation test there is wall condensation in the vessel. By comparing theoretical calculations with experimental deposition rates, we can confirm the reliability of the measured data and provide evidence to clarify the particle mechanisms under various conditions.

$$R(t) = \frac{v_{TS}}{h_s}m(t) + \frac{v_{diff}}{h_{diff}}m(t) + \frac{v_{dph}}{h_{dph}}m(t) + \frac{v_{th}}{h_{th}}m(t) \tag{5}$$

The ELPI+ measures the online current signal of the sampled particles and converts this signal into mass concentration in $\mathrm{g\,m^{-3}}$ by mathematical calculation through equation 6 [20]. Therefore, the uncertainty from the ELPI+ measuring can be estimated following the propagation of uncertainty in equation 7 [21]. The uncertainties of charging efficiency X, Aerodynamic cut-off diameter $D_{a,50}$ and current are 10.8 %, 2 % and 1 %, respectively [22]. The uncertainty of dilution factor comes from slight fluctuation of sampling gas and changes from 1 % to 7 %. Thus, taken into account all of these factors, the total uncertainty of mass concentration measuring is around 12 %.

$$c_m = \frac{1}{X}\frac{\rho_p D_i^3 \pi}{6}\lambda I * 10^{-6} \tag{6}$$

$$u_m = \sqrt{(f'(X)u_X)^2 + (f'(D_i)u_{D_i})^2 + (f'(\lambda)u_\lambda)^2 + (f'(I)u_I)^2} \tag{7}$$

3.1 Temperature influence

We carried out a series of experiments on the effect of temperature on aerosol depletion behavior of both pure substances and their mixtures. The results cast lights on the understanding of aerosol settling phenomena in containment due to the influence of temperature.

3.1.1 Pure substances

The effects of temperature on the depletion behavior of insoluble aerosols was studied with varying heating temperatures RT (around 23 °C), 120 °C and 180 °C. To make the comparison of different relative humidities at high temperatures possible, the temperature variation of the CsI particles are concentrated only at RT and 60 °C. Figure 6 illustrates the results of the investigations on the influence of temperature on the depletion behavior of SnO_2 and CsI particles, respectively. The logarithmic mass concentration (left Y-axis) and aerosol removal rate (right Y-axis) are plotted against depletion time. Solid line represents mass concentration and dash line is corresponding calculated aerosol removal rate. By increasing temperature, the aerosol removal rate of both substances seems to be unchanged ($\lambda_{RT}(t) = \lambda_{hightemperature}(t)$). Therefore, the change of temperature has no impact on the depletion behavior for both particles, regardless if it is soluble or insoluble. The mass concentration decreases with the depletion time. In the first 2 hours, the depletion for both particles appears to be most active, and the mass concentration decreases at an almost constant rate afterwards. The removal rate of SnO_2 is calculated to be 0.63 1/h. After 2 hours depletion, the removal rate of CsI is maintained at 0.26 1/h.

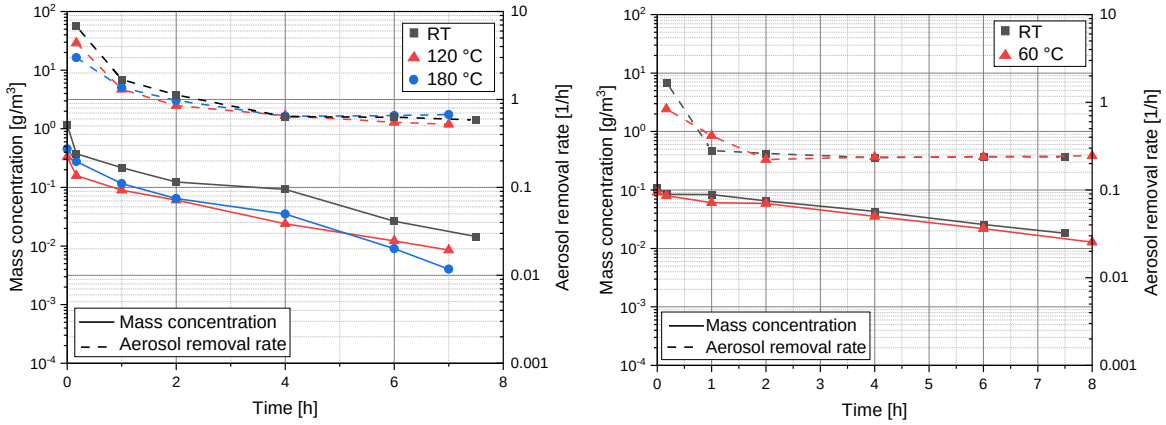

Figure 6: Temperature impact on mass concentration and aerosol removal rate of SnO_2 particles (left) at dry, 3 bar (g) and CsI particles (right) at dry, atmospheric pressure.

Figure 7 gives an overview of the size distribution of SnO_2 and CsI particles at different temperatures. Regardless of the substances, each curve fits very well at the corresponding depletion time, and it seems to have no significant difference due to temperature. During the first 10 minutes of depletion, the size distribution changes significantly for both particles. Submicron particles aggregate to the micron level and the Aerodynamic count median diameter (ACMD) shifts to the right. For SnO_2 particle, ACMD changed from 0.52 µm to 1.16 µm within 8 hours, while it varies from 0.45 µm to 0.98 µm for CsI particle. Obviously, the ACMD of CsI is smaller than that of SnO_2. It is remarkable that after 10 minutes of depletion, the number of micron-sized particles is similar to the injection phase, suggesting that agglomeration is the dominant mechanism in that period. For CsI particle, even until 4 hours of depletion, the number of micron particles is still larger than before. The reason should be, the submicron particles of CsI are more numerous, which enhances the agglomeration. To verify this view, we compared the experimental data and the theoretical values of particle growth due to thermal agglomeration in Figure 8. The data displayed here are measured at RT, the measured ACMD/AMMD/GSD trends are identical at higher temperatures. The function applied is approximately correct for solid particles that describe particle growth due to thermal agglomeration [15]. The coagulation coefficient K is calculated by interpolation from the coagulation coefficient data for polydisperse aerosols. For SnO_2 and

CsI particles, K is calculated to be 5.26 and 5.44. In the case of SnO_2 particle growth, the experimental and theoretical values of ACMD are in good agreement for the first hour, the measured ACMD remains constant afterwards and does not increase as calculated. Theoretical analysis suggests that a stable "self-preserving size distribution" will form after a long time with a GSD of approximately 1.5 [15, 23], which is occurred in IN-EX experiments. For CsI particles, the contribution of agglomeration to particle growth is more pronounced than for SnO_2. The measured ACMD does not increase as calculated until after 4 hours of depletion. For SnO_2 particles, the number concentration has almost no change after 4 hours of depletion. The reason could be the dynamic balance between the agglomeration of submicron particles and the sedimentation of micron particles. It is confirmed that the method of forming a stable particle size distribution is based on the removal of small particles by agglomeration and the removal of large particles by sedimentation [15].

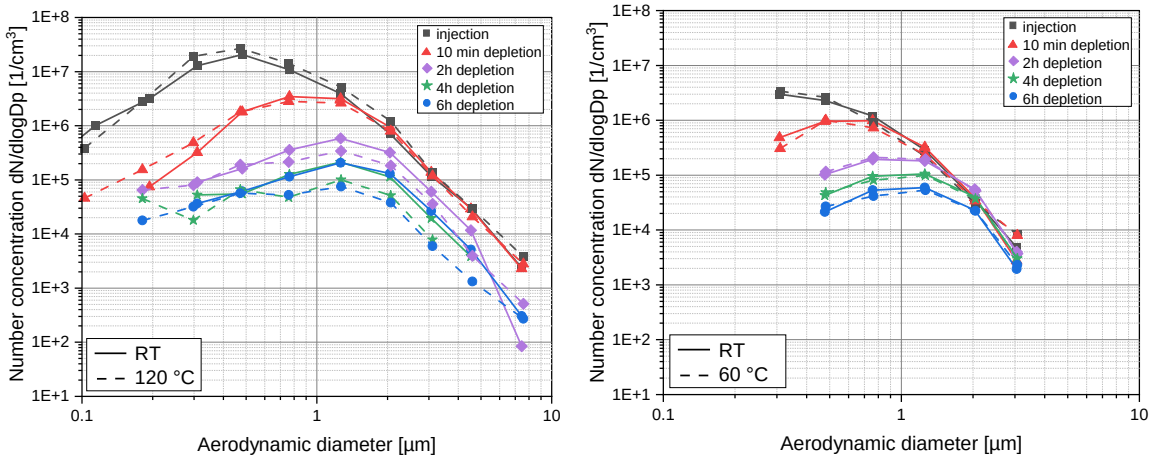

Figure 7: Temperature impact on size distribution of SnO_2 (left) and CsI (right) particles at dry, atmospheric pressure.

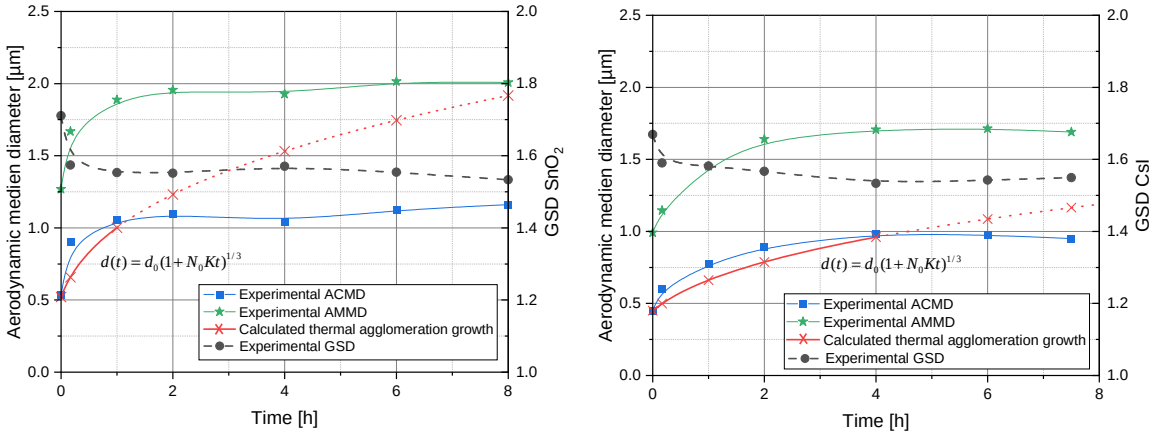

Figure 8: Comparison with theoretical agglomeration particle growth of SnO_2 (left) and CsI (right) particles at RT, dry, atmospheric pressure.

3.1.2 mixture

Considering the effect of temperature on the depletion behavior of the mixture, Figure 9 shows the trend of mass concentration and aerosol removal rate of the mixture with time at two different temperatures, RT and 60 °C. Because we observed the same results in the experiments regardless of the mass composition, the results for 6:4 (CsI:SnO_2) mass fraction are shown here as an example. It shows that the temperature seems to have no impact on mixture depletion ($\lambda_{RT}(t) = \lambda_{hightemperature}(t)$). This view agrees with the conclusion for pure particles. The aerosol removal rate for this mixtures is around 0.32 1/h.

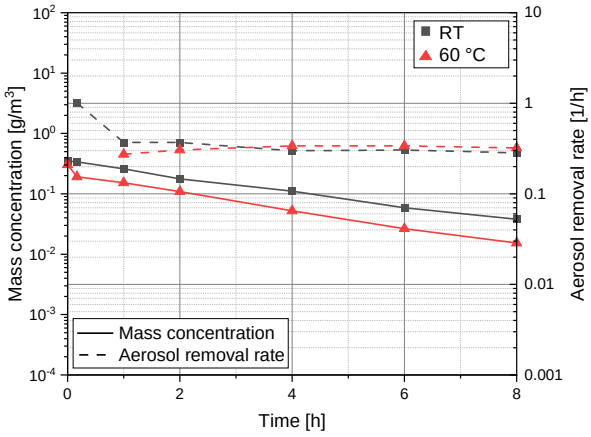

Figure 9: Temperature impact on depletion tendency and aerosol removal rate of mixture with the mass fraction CsI:SnO_2 = 6:4 at medium humidity, atmospheric pressure.

3.1.3 Discussion

According to the results, there is no influence on depletion behavior or size distribution of $SnO2$, CsI and their mixture due to temperature, which ranges from RT to 200 °C in IN-EX experiments. The assumed reason for this is, as temperature increases, the dynamic viscosity of carrier gas would also increase which could slow down the settling. However, as shown in Figure 10, the decrease in theoretical sedimentation deposition rate (dash lines) is slight due to the increase in temperature and this deceleration in depletion can be ignored. Moreover, the activity of molecular and collision frequency will increase due to the increase in temperature. Therefore, thermal agglomeration should also be enhanced, because coagulation coefficient K increases with temperature increasing [15]. For example, for monodisperse particles, if the temperature is increased from RT to 120 °C, the coagulation coefficient K changes from 3.0 x 10^{-10} $cm^3\,s^{-1}$ to 3.2 x 10^{-10} $cm^3\,s^{-1}$. In combination with Smouluchoswski's function, particle growth due to thermal agglomeration is limited at high temperatures [23]. Thus, the results show that temperature changes seem to have no effect on aerosol depletion behavior. It also applies to mixtures. Furthermore, the deposition rate is concentration dependent. To be able to compare deposition rates using measured data at two different temperatures, the initial mass concentration at RT is to be regarded as the standard. The calculated theoretical deposition rates are higher than the experimental values at the beginning of depletion for both SnO_2 and CsI, and the deviation decreases with depletion time (see Figure 10). The calculated sedimentation rate is overestimated, as all small particles are considered to be settled during the sedimentation calculations, but in fact a large amount of them form large particles due to agglomeration. The agglomeration effect of CsI particles is stronger than that of SnO_2 particles.

3.2 Pressure influence

There are very few experiments focusing on the pressure impact on aerosol depletion and there is little understanding about the pressure influence. The IN-EX experiments can simulate the actual thermal hydraulic conditions of the containment. Thus, the results can provide more information about the influence of pressure on aerosol depletion, and it clarifies a comprehension of the pressure impact.

3.2.1 Pure substances

Pressure varies from atmospheric pressure, 3 bar (g) and 6 bar (g) in the experiments. Due to the difference regarding particle losses between the two diluters, comparison of particle depletion results between atmospheric pressure and high pressure should be done carefully. Figure 11 illustrates the results of pressure impact on the SnO_2 and CsI depletion behavior. The aerosol removal rate is highly uniform at different pressures for both particles. After 4 hours of depletion, the aerosol removal rate of SnO_2 changes to a constant 0.63 1/h. While after 1 hour of depletion, the aerosol removal rate of CsI remains at 0.48 1/h. The removal rates measured at high pressures are not the same as those at atmospheric

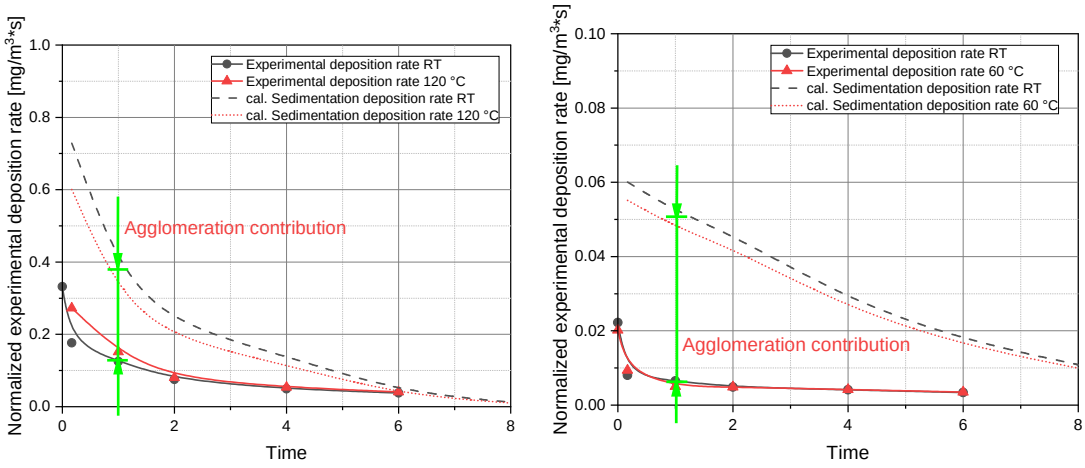

Figure 10: Comparison with theoretical sedimentation deposition rate of SnO_2 (left) and CsI (right) particles at dry, atmospheric pressure.

pressure. As mentioned previously, the diluter DEED-300 applied under high pressure conditions is different from the diluter DI-2000 at atmospheric pressure in IN-EX experiments. It is not meaningful to compare the data using DEED-3000 with the data using DI-2000 (at atmospheric pressure). It may lead to differences in measurements and thus to incomparable aerosol removal rates. However, comparisons using the same dilutors DEED-3000 at 3 bar (g) and 6 bar (g) can yield information on the effects of pressure, as shown in Figure 11. It shows that the variation of pressure seems to have no influence on the SnO_2 and CsI aerosol depletion ($\lambda_{3bar}(t) = \lambda_{6bar}(t)$).

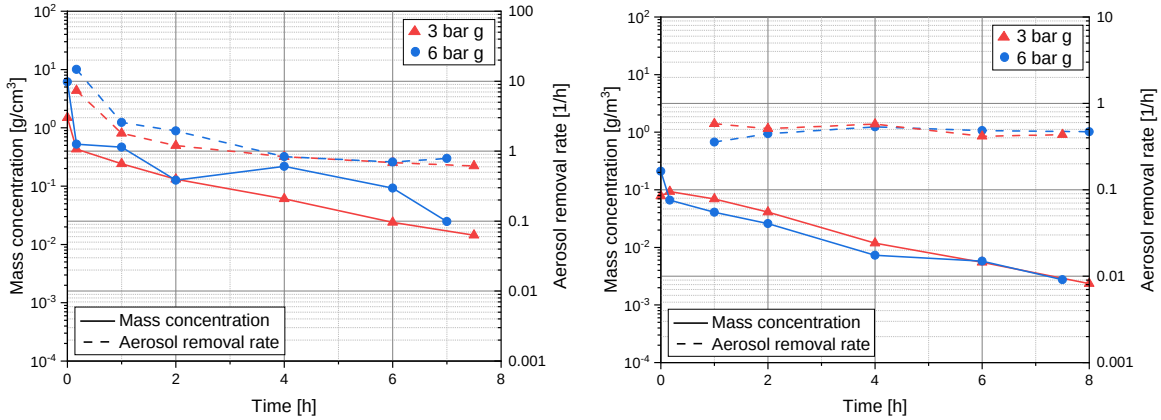

Figure 11: Pressure impact on mass concentration and aerosol removal rate of SnO_2 (left) and CsI (right) particles at RT, dry.

To verify the results of pressure impact, complementary experiments were conducted. Considering the decrease in pressure during the measurement, the number of measurements was reduced from 7 to 3 and in some cases even 2 during the entire depletion time (8 hours). Then, the results could be obtained for different pressures at the same depletion time points, as presented in Figure 12. We also obtained the same results from the complementary experiments of SnO_2. Here is an example of the experiment of CsI to explain the results. In one of the complementary experiments, only 2 measurements (4 hours and 6 hours of depletion) were carried out. The corresponding measurement pressures (4.2 bar and 3.8 bar) were higher than usual (3.1 bar and 2.8 bar) at the time of measurement. Similarly, in another experiment, only the depletion time of 8 hours was measured. There is almost no difference of aerosol removal rate between each depletion time point at different pressures. Therefore, the pressure drop during the measurement has no effect on the results.

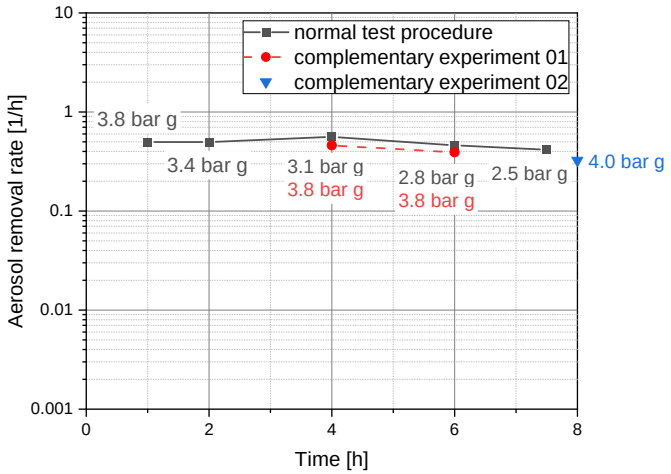

Figure 12: Pressure impact on CsI depletion at RT, 3 bar (g), medium humidity.

Focusing on the size distribution of SnO_2 and CsI particles at two different high pressures in Figure 13. For both particles, the size distribution curves appear to be parallel over the depletion time. Within 2 hours of depletion, the changes in number concentration of SnO_2 and CsI due to pressure show consistency. The higher the pressure, the higher the measured initial injection number concentration. It should be noted that the dilutor DEED-300 is used to depressurize high-pressure samples to atmospheric pressure. These data are measured at atmospheric pressure. The data shown in the graphs are recalculated data which were converted from the measured data from atmospheric pressure to the expected pressure. Based on the ideal gas equation, the concentration becomes higher in the circumstance of high pressure. After 4 hours of depletion, the size distributions between the two pressures display differences or inaccuracy. This is because the concentration of particles in the vessel are quite low at later stages of depletion, and after dilution, the measured particle concentration is even lower, possibly below the detection threshold of ELPI+.

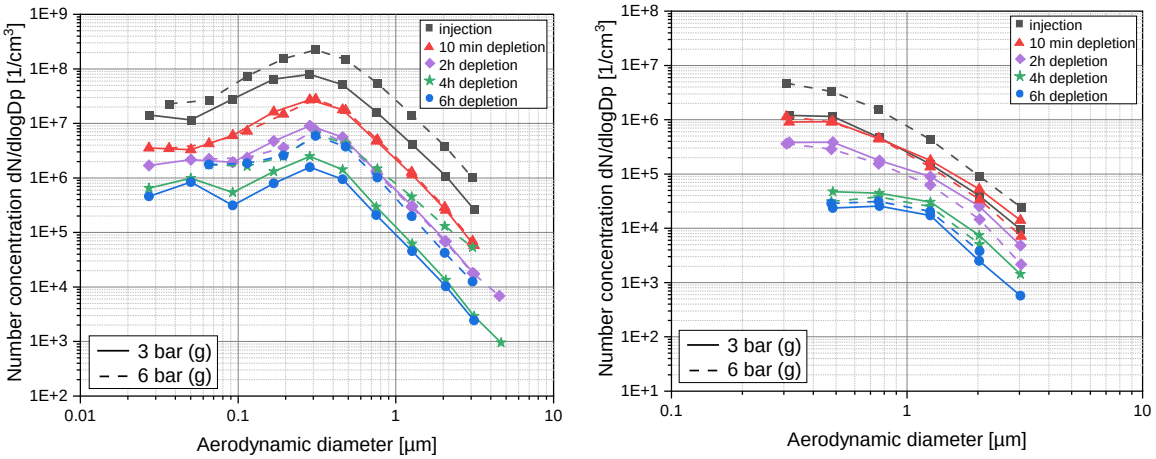

Figure 13: Pressure impact on size distribution of SnO_2 (left) and CsI (right) particles at RT, dry.

Figure 14 compares measured ACMD/AMMD/GSD with theoretical particle growth due to thermal agglomeration at RT, dry and 3 bar(g) conditions. For the SnO_2 particles (left side of the graph), the coagulation coefficient K is interpolated to be 6.2 x 10^{-10} $cm^3\,s^{-1}$. There was no particle growth observed under high pressure conditions, and it is considerably different from the expectation of agglomeration. It appears that, at least for SnO_2 particles, agglomeration is suppressed under high pressure. From another point of view, the agglomeration and sedimentation rates reach an balance. The loss of small particles due to agglomeration equals the loss of large particles due to sedimentation, therefore keeping ACMD/AMMD/GSD constant. For CsI particles (right side of the graph), the coagulation coefficient K

is interpolated to be 5.7 x 10^{-10} $cm^3 s^{-1}$. The particle growth of ACMD is basically consistent with the expectation of thermal agglomeration at first 4 hours. As time passes, agglomeration narrows the size distribution and the GSD decreases with time until a stable 'self-preserving size distribution' as around 1.5. At high pressure, the calculated GSD declines from 2.0 to 1.6 during 6 hours depletion. CsI agglomeration at high pressure appears to be the same as at atmospheric pressure.

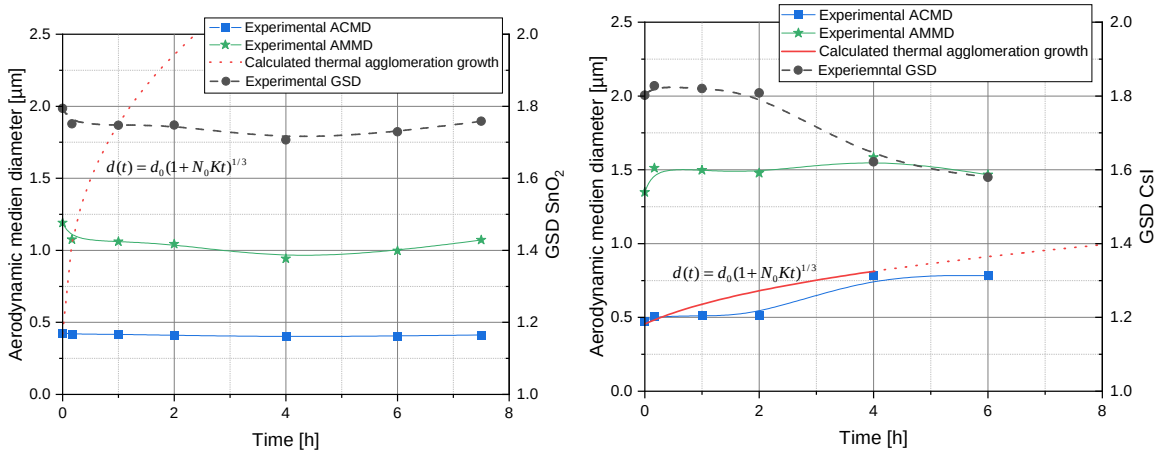

Figure 14: Comparison with theoretical agglomeration particle growth of SnO_2 (left) and CsI (right) particles at RT, dry, 3 bar(g).

3.2.2 Mixture

Turning to the influence of pressure on the depletion of multi-components aerosols, we take Figure 15 to display the trends of mass concentration and aerosol removal rate at 3 bar (g) and 6 bar (g). Since we obtained the same results regardless of mass composition, 3:7 mass fraction of CsI and SnO_2 are used as an example to explain the results. There is almost no difference in the aerosol removal rate curves. As with pure particles, pressure has no effect on the depletion behavior of the mixture ($\lambda_{3bar}(t) = \lambda_{6bar}(t)$).

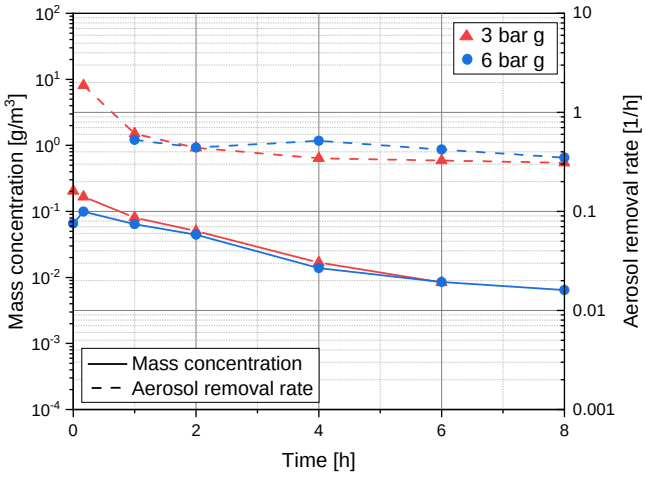

Figure 15: Pressure impact on depletion tendency and aerosol removal rate of mixture with the mass fraction CsI:SnO_2 = 3:7 at RT, medium humidity.

3.2.3 Discussion

The variation of pressure seems to have no influence on the depletion behavior of SnO_2, CsI and their mixture. As the pressure increases, the dynamic viscosity of carrier gas increases and slip correction factor Cc decreases. These changes slightly decelerates the settling of particles. Nonetheless, the caused effect is mostly negligible. As shown in Figure 16, the calculated theoretical settling rates are

almost identical at both pressures. For SnO_2 particles, the measured deposition rates were in close agreement with theoretical sedimentation expectations, and no contribution from agglomeration was observed. Whether agglomeration is suppressed or there is an equilibrium between agglomeration and sedimentation to explain this phenomenon, we need further experimental and analytical methods to figure it out. For CsI particles, the comparison of deposition rates between experiments and theoretical calculation at both pressures is similar to the effect of temperature mentioned earlier. Small particles first aggregate into larger particles which are actually included in the sedimentation rate calculation, so the experimental deposition rate for CsI is less than the sedimentation expectation, the theoretical calculation is overestimated.

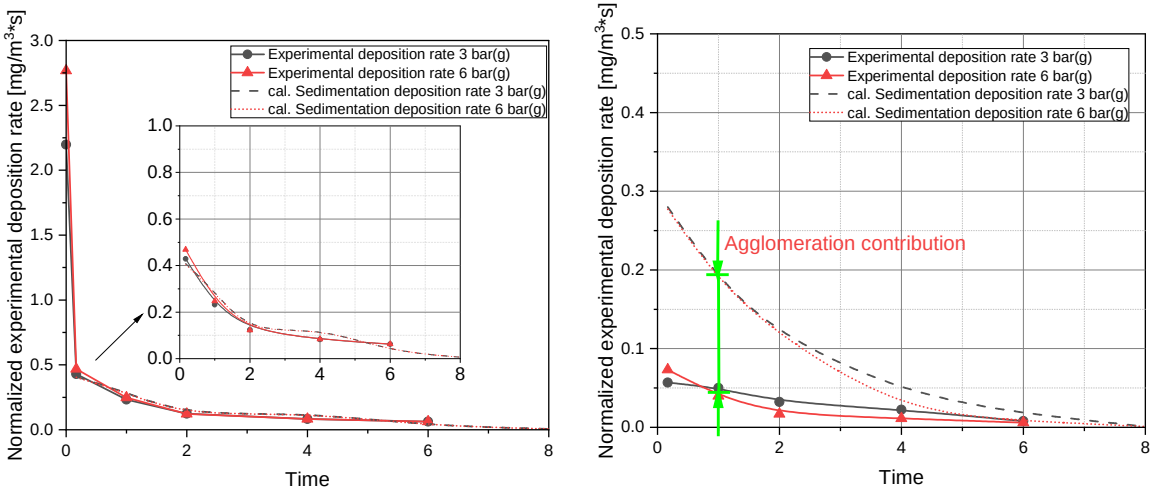

Figure 16: Comparison with theoretical sedimentation deposition rate of SnO_2 (left) and CsI (right) particles at RT, dry condition.

3.3 Relative humidity influence

Experiments on the impact of relative humidity on the depletion behavior of pure aerosols (SnO_2 and CsI) and their mixture in the IN-EX vessel were performed at different humidity conditions, including fog and volumetric condensation. It should be noted that reaching a high humidity at high temperatures is very difficult due to the limitations of the steam generator. Therefore, the condensation tests could only be conducted under room temperature.

3.3.1 Pure substances

Figure 17 illustrates that the depletion behavior of SnO_2 and CsI particles under the influence of humidity. For SnO_2 on the left side, the aerosol removal rate keeps constant with increasing relative humidity after 2 hours($\lambda_{RH1,SnO_2} = \lambda_{RH2,SnO_2}$). The depletion behavior of SnO_2 particles seems to be independent of humidity. There is no difference in the impact of ambient humidity or the volume condensation on the deposition of these particles. Only in the first 2 hours the depletion seems to differ for different humidity levels because no measurement for the 1 hour depletion at condensation was carried out. The aerosol removal rate decreases with depletion time from 2.03 1/h to 0.55 1/h over 8 hours. After 4 hours of depletion, the removal rate remains approximately constant. For CsI on the right side, the mass concentrations show almost no differences at dry and medium humidity conditions. The mass concentration at condensation, especially the initial value, is much lower than the mass concentration in other circumstances. In terms of the aerosol removal rate, the higher the relative humidity, a faster aerosol removal rate for CsI particles could be observed. The removal rate of the particles at condensation is the fastest. At high humidity, water droplets may be present in the system due to the hygroscopic properties of CsI particles. The nucleated condensation may occur. Therefore, the removal rate is close to the case of condensation.

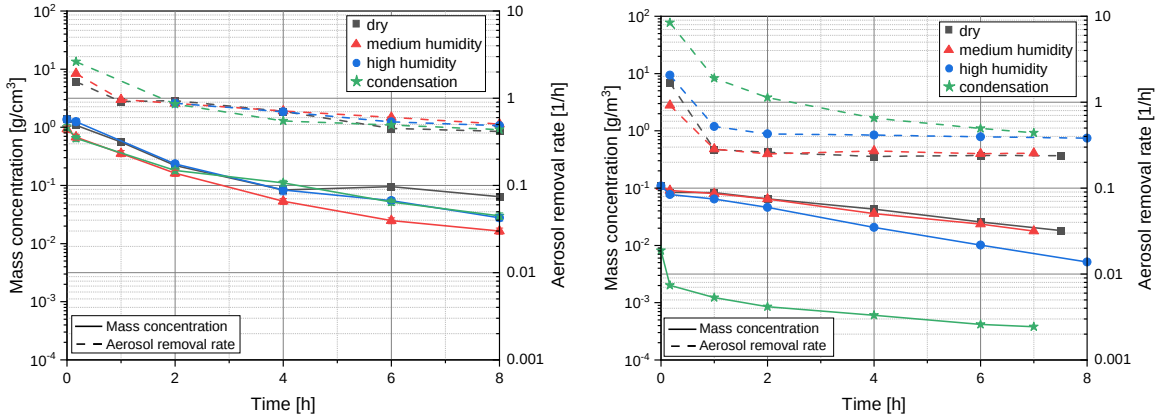

Figure 17: Relative humidity impact on mass concentration and aerosol removal rate of SnO_2 (left) and CsI (right) particles at RT, atmospheric pressure.

In addition to the change in mass concentration, the size distribution of SnO_2 and CsI particles during depletion is plotted in Figure 18. It seems that humidity has no impact on size distribution for SnO_2 particles. In contrast, the size distribution of CsI particles differs considerably under the two humidity conditions. In the case of condensation, the initial size distribution is much lower than that at medium humidity, especially for micron-sized particles. This could be explained by the fact that a drastic settling of particles occurs during the injection phase. Due to the surface tension of the water droplets, a large amount of CsI particles adhere to the surface due to its hydrophilic property and settle down with the gravity of water droplets. After injection, the rate of agglomeration and sedimentation rapidly enters dynamic equilibrium because there is no source of water droplets.

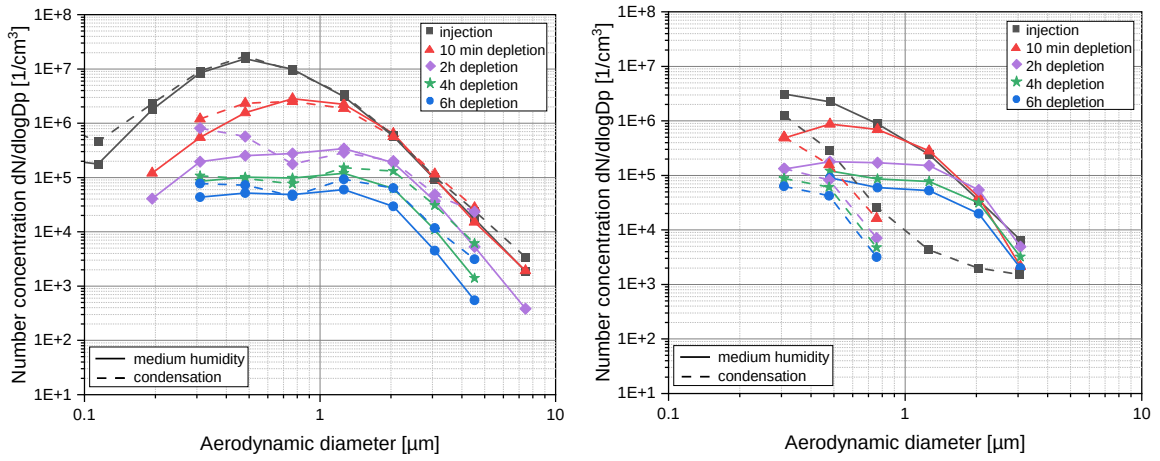

Figure 18: Relative humidity impact on size distribution of SnO_2 (left) and CsI (right) particles at RT, atmospheric pressure.

3.3.2 Mixture

From the experimental results of pure substances, for CsI, the higher the relative humidity, the faster the aerosol removal rate. The aerosol removal rate reaches the upper limit of condensation. Since the influence of relative humidity on these two aerosol species is different, the results of the mixtures with different mass fractions should be divided for analysis. Figures 19 show the trends of mass concentration and aerosol removal rate for mixtures of different mass compositions at different relative humidity conditions. It is observed that there is no difference in the aerosol removal rate for a mass fraction of CsI and SnO_2 of 3:7, and the same conclusion is reached in the experiments for the insoluble particle SnO_2. However, for a mass fraction of CsI and SnO_2 of 6:4, the removal rate indicates a regular increase with increasing relative humidity, which is the same result as in the experiments with pure CsI.

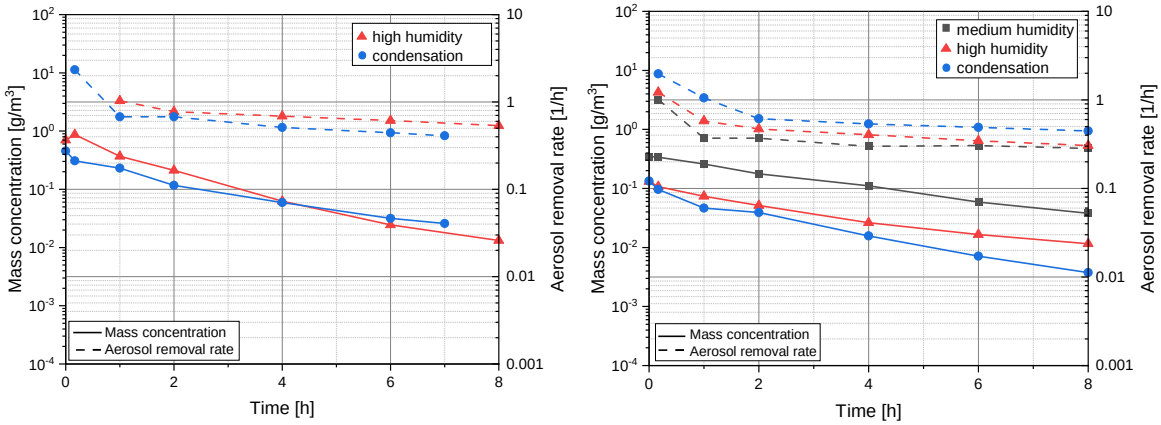

Figure 19: Humidity impact on depletion tendency and aerosol removal rate of mixture with the mass fraction CsI:SnO_2 = 3:7 (left) and 6:4 (right) at RT, atmospheric pressure.

3.3.3 Discussion

There seems to be no impact of relative humidity, regardless of mist condition or volume condensation, on the depletion behavior and size distribution of insoluble SnO_2 aerosols in general ($\lambda_{RH1,SnO_2} = \lambda_{RH2,SnO_2}$). For CsI, the higher the relative humidity, the faster the aerosol removal rate. It seems to have the highest aerosol removal rate in case of condensation. Combining the results for pure substances of SnO_2 and CsI, it appears that higher relative humidity favors the depletion of soluble aerosols. This is in agreement with Allelein et al. [1]: condensation may occur even in the case of unsaturated state for hydrophilic substances. To verify the reliability of the measured data for CsI particles at different humidity conditions. Figure 20 compares with the hygroscopic growth factors from G. Mishra et al. [24, 25] at different relative humidities. The relative humidity is plotted as a qualitative value for comparison as the control of relative humidity in the IN-EX test was not precise. These data are in good agreement under mist conditions. However, comparable data are not available in condensation conditions by G. Mishra et al.. Another reason for the different influence of relative humidity on SnO_2 and CsI might be the size of steam molecular is generally submicron or smaller, which is beneficial to agglomeration and diffusion [15, 26] for both particles. However, as far as CsI particles are concerned, they are mostly submicron particles. Therefore, aerosol agglomeration dominates the aerosol depletion for CsI, as mentioned previously. It takes relatively longer time for the agglomeration and sedimentation rates to reach equilibrium during depletion, whereas for SnO_2 particles, gravitational settling plays a dominant role in the aerosol depletion. The acceleration for agglomeration due to steam could be ignored, comparing to the sedimentation effect on the depletion. Therefore, the effect of humidity on CsI is more significant.

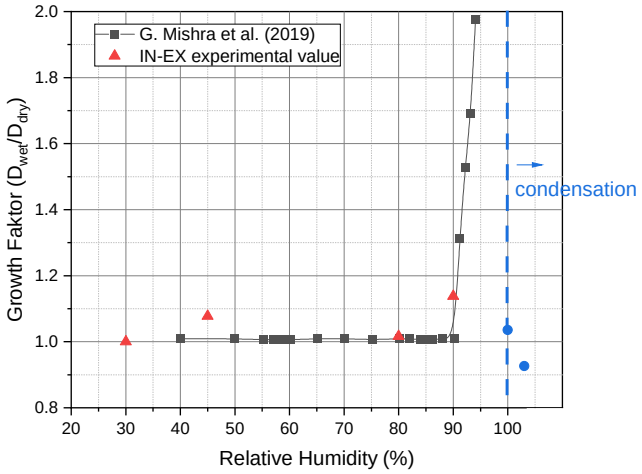

Figure 20: Comparison of the relative humidity growth factors for CsI of IN-EX and the literature.

It is remarkable that the depletion behavior for CsI particles at condensation is different. Figure 21 describes the differences among AMMD, ACMD, and GSD for CsI particles at medium humidity and condensation conditions. The understanding for the CsI depletion at mist condition is similar to the temperature and pressure effects mentioned earlier. However, in the condensation scenario, the ACMD remains constant throughout the depletion process, suggesting that agglomeration does not affect depletion in this case. The sudden drop in AMMD and GSD after injection indicates that there is significant large particles' loss, which narrows the size distribution. Besides agglomeration and sedimentation influences, the effects of wall condensation should also be taken into account in the case of condensation, as the heating temperature in the vessel was only 60 °C. According to the results, the wall condensation plays a crucial role in reducing the initial concentration of particles. Furthermore, due to the surface tension of water droplets, submicron particles would adhere to the surface of water droplets in the occurrence of volume condensation, which in turn accelerates the settling [15, 27]. Due to the hydrophilicity of CsI particles and their size distribution, it is more sensitive to change in humidity. In the case of condensation, wall condensation, agglomearation and sedimentation combine to complicate the depletion behavior. Discussing the effect of humidity on the depletion behavior of multi-component aerosols, it concludes that the depletion behavior of the mixture is close to that of the main components in the mixture.

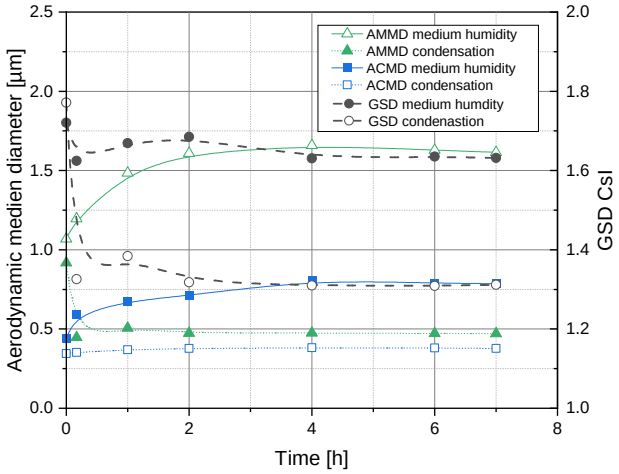

Figure 21: Comparison of CsI particle growth between medium humidity and condensation at RT, atmospheric pressure.

3.4 Mass composition influence

The comparison between pure particles and mixtures (mass composition influence) is essential to obtain regularities in the depletion behavior. This is vital to clarify how nuclear aerosols change in practice, and it extends the understanding of accident aerosols during depletion. Figure 22 shows the tendency of mass concentration and aerosol removal rate varying with mass composition. Looking closer at the mass concentration at medium humidity, SnO_2 has the steepest curve and fastest aerosol removal rate. The rest of the curves appear to be parallel, and it is difficult to distinguish which is faster and which is slower. However, the tendency of aerosol removal rate answers this question. It is clear that CsI has the smallest aerosol removal rate and SnO_2 has the highest aerosol removal rate. The greater the composition of SnO_2 in the mixture, the faster the depletion. In the condensed state, the aerosol removal rate seems to be the same for the pure substance and the mixture. This implies that water droplets play a crucial role in the depletion regardless of the aerosol substances. Other mechanisms such as agglomeration have a very limited effect on depletion in this case.

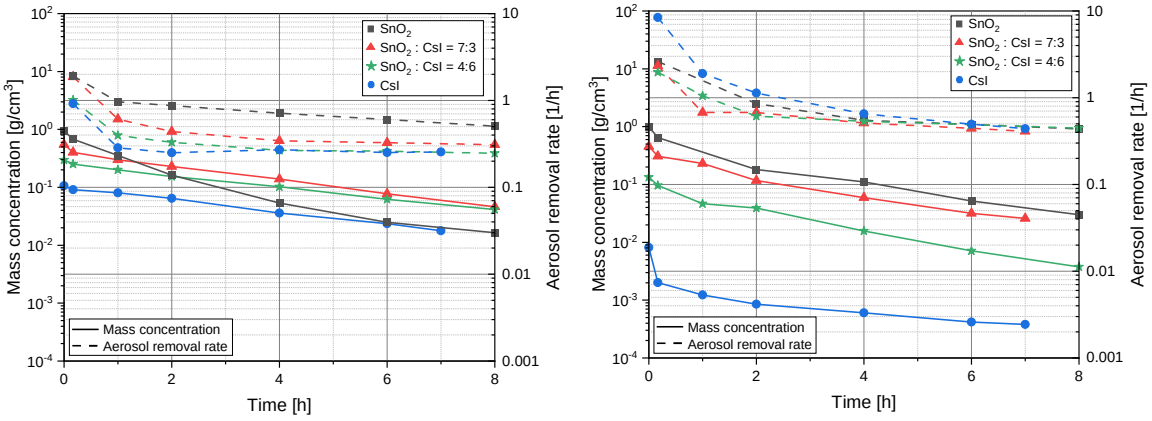

Figure 22: Comparison of results on mass concentration and aerosol removal rate for pure substance and mixture at RT, atmospheric pressure, medium humidity (left) and condensation (right).

3.5 Comparison with KAEVER

Similar experiments were performed in the KAEVER project in 1997 to study the behavior of aerosol depletion. Unlike the IN-EX experiments, in the KAEVER experiments only the impact of relative humidity on aerosol depletion was studied. However, the KAEVER project investigated various insoluble (SnO_2, Ag) and soluble substances (CsI, $CsOH$). It provided a range of data and made it possible to compare the results. The KAEVER test facility is a prototype test model of a nuclear reactor containment vessel. The vessel has an internal free volume of 10.595 m^3 [6, 7, 8, 9], which is ten times larger than the IN-EX vessel. Therefore, the mass concentrations in KAEVER and IN-EX are not of the same order of magnitude. To make the comparison possible, we have drawn the diagram 23 in KAEVER's way and our way respectively. First in the way of KAEVER (left side of Figure 23), we recalculated IN-EX data from comparable experiments (CsI depletion at dry condition) at standard temperature and pressure (STP) and shifted the data to the right along the X-axis to find similar and comparable mass concentrations of KAVER. This suggests that if the mass concentration of IN-EX is the same as that of KAEVER, they have similar depletion curves. Then the KAEVER data have been recalculated as aerosol removal rate and plotted over the right side of Figure 23, thus eliminating the effect of the initial mass concentration and emphasizing the rate of mass concentration change. The results shows that the aerosol removal rate of CsI by IN-EX is less then KAEVER under dry conditions, the reason could be the different volumes of the measured vessels.

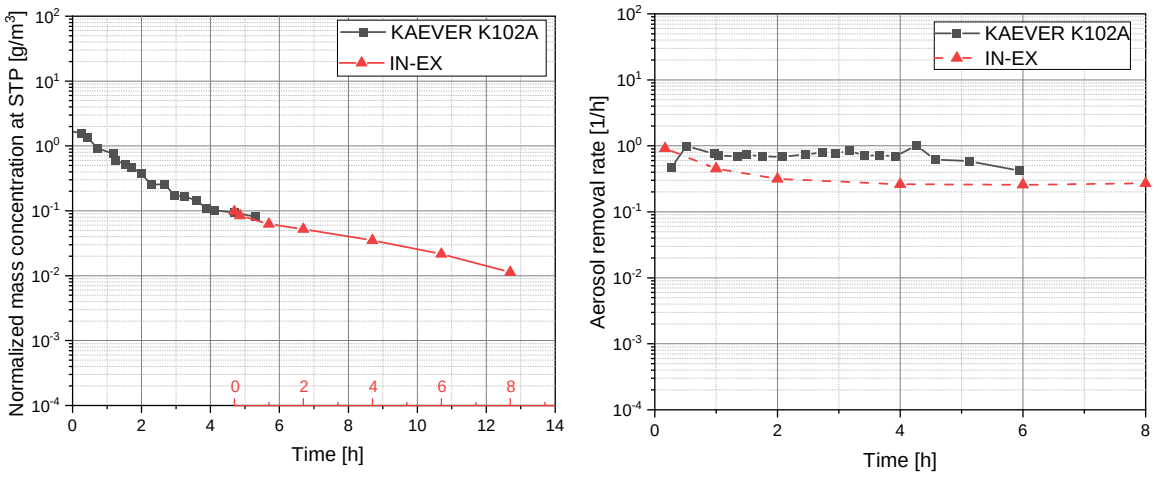

Figure 23: Results comparison between IN-EX and KAEVER in different way at STP for CsI depletion at dry condition.

Figure 24 compares the depletion behavior between IN-EX and KAEVER experiments under different humidity conditions. In case of high humidity, the compared KAEVER experiments (K131 and

K138) were both performed at 120 °C, high humidity and 3 bar (g). However, the IN-EX experiments were not conducted under these conditions. According to the IN-EX experiments, temperature and pressure have no effect on the depletion of SnO_2. Even so, we chose a SnO_2 result under atmospheric conditions and normalized the data at STP for comparison with KAEVER and hence to verify IN-EX conclusions. Besides, since KAEVER also tests the depletion behavior of Ag particles, which are representative particles for the core melt aerosols as well, it provides the possibility to compare the results between different insoluble aerosols. It is shown that after 1 hour of depletion, the aerosol removal rate match each other quite well, regardless of particle species. Their aerosol removal rate is generally identical, with about 0.63 1/h. However, the trends of increasing forward then decreasing afterwards in KAEVER was not observed in IN-EX results. This might be due to different test procedures or different particle size distributions provided by the aerosol generators between IN-EX and KAEVER. We also compared the results of IN-EX and KAEVER (K151 and K159) for different aerosols (SnO_2, CsI and Ag) under condensation conditions (the right side of Figure 24). For the same reason, we chose to compare the results with KAEVER under similar conditions after normalizing at STP, even though the boundary conditions among the comparable results are not the same. This comparison is worthy enough to confirm the IN-EX arguments: the aerosol removal rate seems to be the same for different kinds of particles at condensation, respectively.

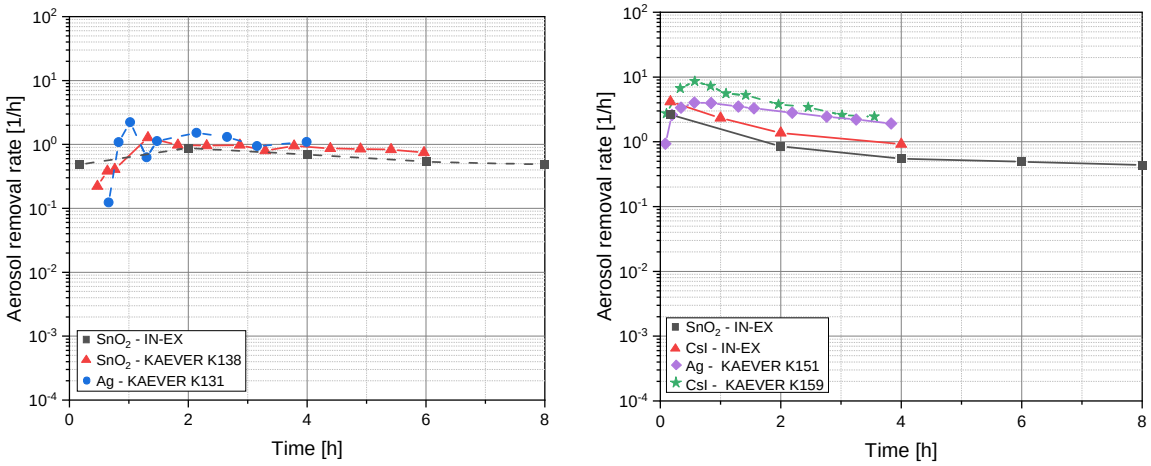

Figure 24: Results comparison between IN-EX and KAEVER for aerosol removal rate at high humidity (left) and condensation (right) after normalizing at STP.

4 Conclusion

In the IN-EX experiments, we provide a novel approach to compare the depletion behavior, in particular the aerosol removal rate, for different initial mass concentration scenarios and we obtain some conclusions regarding the depletion behavior of pure and multi-component aerosols influenced by thermodynamic parameters as follows:

- Temperatures varying from room temperature to 180 °C seem to have no impact on depletion and size distribution of SnO_2, CsI and their mixed aerosols. In these cases, the acceleration due to thermal agglomeration and the deceleration to sedimentation seem to be in balance.
- Pressures ranging of atmospheric pressure up to 6 bar (g) seem to have no influence on the depletion of CsI and SnO_2 particles, and it shows no impact on their mixtures depletion either. According to the results of size distribution, we observed that there are more sub-micron SnO_2 particles at higher pressure. We assume that the high pressure can suppress agglomeration for insoluble particles. It needs more experiments to verify.
- For relative humidity, there is no impact on the depletion behavior and size distribution of insoluble SnO_2 aerosols, regardless of mist condition or volume condensation. While for CsI, the higher

the relative humidity, the faster the aerosol removal rate. It has the highest aerosol removal rate in case of condensation, it has been already observed in previous test series. Moreover, the depletion behavior of the mixture is close to that of the main components in the mixture. If the composition of SnO_2 dominates, then the humidity has only slightly effect on the depletion of the mixture. On the other hand, if the mass fraction of CsI in the mixture is higher, then the aerosol removal rate increases with increasing humidity. However, the cut-off for the mass composition between SnO_2 and CsI is not clear.

- SnO_2 has the fastest aerosol removal rate. The greater the composition of SnO_2 in the mixture, the faster the depletion velocity. The depletion of CsI is the slowest under all conditions. In particular, under condensation conditions, the aerosol removal rate is the same for SnO_2, CsI and their mixture. The wall condensation and sedimentation of water droplets plays a dominant role.
- The findings of IN-EX experiments were further confirmed by comparison with the KAEVER experiments, in this case, the ratio of test vessel surface and volume does not have any impact on the overall depletion behavior, but it has to be checked if it applies in general. The agreement with the KAEVER Ag results suggests that the IN-EX findings can be extended to other aerosols, at least insoluble ones.

For further work, the corresponding correlations of time-dependent aerosol removal rate will be derived. More experiments need to be performed to figure out the pressure impact on the size distribution. To understand the aerosol mechanisms more, the experiments on the interaction effect among multi-component aerosols (the mixture of CsI, Cs_2MoO_4, SnO_2 and Ag) will be conducted.

Acknowledgment

Parts of the work presented in this paper are funded by the German Federal Ministry for the Environment, Nature Conservation, Nuclear Safety and Consumer Protection (BMUV, grant No. 1501551) on the basis of a decision by the German Bundestag.

References

[1] H. J. Allelein et al. “State of the art report on nuclear aerosols”. In: *CSNI Report* (2009).

[2] A. Fromentin et al. “Demona (Demonstration of Nuclear Aerosol Behavior) - Study of Aerosol Behavior in a Containment”. In: *Journal of Aerosol Science* 19.1 (1988), p. 65. ISSN: 0021-8502.

[3] K. Fischer and T. Kanzleiter. “Experiments and computational models for aerosol behaviour in the containment”. In: *Nuclear Engineering and Design* 191.1 (1999), pp. 53–67. ISSN: 0029-5493.

[4] T. Kanzleiter et al. “The Vanam Experiments M1 and M2 - Test-Results and Multicompartmental Analysis”. In: *Journal of Aerosol Science* 22 (1991), S697–S700. ISSN: 0021-8502.

[5] M. Firnhaber et al. *International standard problem ISP37: VANAM M3 - A Multi compartment aerosol depletion test with hygroscopic aerosol material: comparison report*. Report. 1996.

[6] M Firnhaber et al. *International Standard Problem ISP44-KAEVER-Experiments on the Behavior of Core-melt Aerosols in a LWR Containment Comparison Report*. Report. Organisation for Economic Co-Operation and Development-Nuclear Energy Agency, 2002.

[7] Sture Nordlinder. *International Standard Problem ISP44-Calculation of Aerosol Depletion*. Report STUDSVIK-ES–01-30. 2001.

[8] H.G. Scheibel; G. Poss; D., and Weber. “Influence of aerosolparameters on the aerosol behaviour in reactor containments- first results of the project kaever”. In: *J.Aerosol Sci* 24 (1993), S305–S306.

[9] H.G. Scheibel; G. Poss; and D. Weber. “Kaever: an experiment for an improved understanding of aerosol depletion processes in a reactor containment”. In: *J.Aerosol Sci.* 23 (1992), S209–S212.

[10] B. J. Lewis et al. “Overview of experimental programs on core melt progression and fission product release behaviour”. In: *Journal of Nuclear Materials* 380.1-3 (2008), pp. 126–143. ISSN: 00223115.

[11] T. Haste, F. Payot, and P. D. W. Bottomley. “Transport and deposition in the Phebus FP circuit”. In: *Annals of Nuclear Energy* 61 (2013), pp. 102–121. ISSN: 0306-4549. DOI: 10.1016/j.anucene.2012.10.032.

[12] M. P. Kissane. “On the nature of aerosols produced during a severe accident of a water-cooled nuclear reactor”. In: *Nuclear Engineering and Design* 238.10 (2008), pp. 2792–2800. ISSN: 0029-5493.

[13] H. J. Allelein, C. Kubelt, and E. A. Reinecke. “Impact of cable fire products on severe accident processes”. In: *Proceedings of 2017 international congress on advances in nuclear power plants (ICAPP2017)*, p. 2573.

[14] B. Krupa et al. “IN-EX Facility – Qualification of Measurement Devices under Ther-mophysical Boundary Conditions inside a LWR Containment in the Course of a Severe Accident”. In: *ICAPP 2019 – International Congress on Advances in Nuclear Power Plants*.

[15] William C Hinds. *Aerosol technology: properties, behavior, and measurement of airborne particles*. John Wiley & Sons, 1999. ISBN: 0471194107.

[16] G. Weber H. Nowack C. Spengler S. Schwarz D. Eschricht S. Beck W. Klein-Heßling S. Arndt. *COCOSYS V2.4 User’s Manual*. Gesellschaft für Anlagen- und Reaktorsicherheit (GRS) mbH, 2010.

[17] J. Keskinen, K. Pietarinen, and M. Lehtimaki. “Electrical Low-Pressure Impactor”. In: *Journal of Aerosol Science* 23.4 (1992), pp. 353–360. ISSN: 0021-8502.

[18] Michael Epstein and Phillip G Ellison. “Correlations of the rate of removal of coagulating and depositing aerosols for application to nuclear reactor safety problems”. In: *Nuclear Engineering and Design* 107.3 (1988), pp. 327–344. ISSN: 0029-5493.

[19] C. N. Davies. *Aerosol science*. London, New York: Academic Press, 1966.

[20] *ELPI+ User Manual version1.12*. Dekati Ltd., 2011.

[21] J. Lee et al. “Experimental study on aerosol scrubbing efficiency of self-priming venturi scrubber submerged in water pool”. In: *Annals of Nuclear Energy*. Vol. 114, pp. 571–585. ISBN: 0306-4549.

[22] A. Järvinen et al. “Calibration of the new electrical low pressure impactor (ELPI+)”. In: *Journal of Aerosol Science* 69 (2014), pp. 150–159. ISSN: 00218502.

[23] K. W. Lee. “Change of particle size distribution during Brownian coagulation”. In: *Journal of Colloid and Interface Science* 92.2 (1983), pp. 315–325. ISSN: 0021-9797.

[24] G. Mishra et al. “Hygroscopic growth of CsI and CsOH particles in context of nuclear reactor accident research”. In: *Journal of Aerosol Science* 132 (2019), pp. 60–69. ISSN: 0021-8502. DOI: 10.1016/j.jaerosci.2019.03.008.

[25] G. Mishra et al. “Interaction of cesium bound fission product compounds (CsI and CsOH) with abundant inorganic compounds of atmosphere: Effect on hygroscopic growth properties”. In: *Journal of Hazardous Materials* 418 (2021). ISSN: 0304-3894. DOI: ARTN12635610.1016/j.jhazmat.2021.126356.

[26] Kari E. Lehtinen. *Theoretical studies on aerosol agglomeration processes*. Technical Research Centre of Finland, 1997. ISBN: 9513850471.

[27] G. A. Pertmer and S. K. Loyalka. “Gravitational Agglomeration of Aerosols”. In: *Transactions of the American Nuclear Society* 27.Nov (1977), pp. 618–620. ISSN: 0003-018x.